Chemical Engineering Journal 481 (2024) 148326

Contents lists available at ScienceDirect

Chemical Engineering Journal

journal homepage: www.elsevier.com/locate/cej

CO_2 dissociation using a lab-scale microwave plasma torch: An experimental study in view of industrial application

Christian Karl Kiefer [a,*], Rodrigo Antunes [a], Ante Hecimovic [a], Arne Meindl [a], Ursel Fantz [a,b]

[a] Max Planck Institute for Plasma Physics, Boltzmannstraße 2, Garching, 85748, Germany
[b] AG Experimentelle Plasmaphysik, University of Augsburg, Augsburg, 86135, Germany

ARTICLE INFO

Keywords:
Energy efficiency
Plasma-based CO_2 conversion
Carbon capture and utilization
Wall-plug efficiency
Impurities

ABSTRACT

Under laboratory conditions, microwave plasma torches are known to be an energetically very efficient CO_2 conversion technology, for pressures ranging from 100 mbar up to atmospheric pressure. However, issues relevant for industrial application such as the total energy efficiency, including the power consumption of peripheral equipment, the performance for impure CO_2 streams (such as directly from carbon capture facilities) and the stability at long-term operation are usually not addressed. To fill that gap, a lab-scale plasma torch and the corresponding vacuum pump are connected to an energy meter system. Measured wall-plug energy efficiencies yielded values up to 17.9%, corresponding to an electrical power consumption of 19.6 kWh per produced Nm^3 of carbon monoxide. Experiments with controlled amounts of impurities (Ar, N_2, O_2, real air and synthetic air) in the feed gas stream are performed. It is shown that small amounts of nitrogen can even increase energy efficiency whereas humidity in the CO_2 stream might have an extremely detrimental effect on CO_2 decomposition. Finally, a durability test over 29 h was performed, demonstrating that microwave plasma torch operation is very reproducible and stable in all figures of merit with short ramp-up times, making it a promising technology for intermittent operation on industrial scale.

1. Introduction

Carbon dioxide concentration in the atmosphere is continuously rising, and even the growth rate shows no signs of a soon decrease of atmospheric CO_2 concentration (+2.5 ppm/yr in 2019 [1], +2.4 ppm/yr in 2020 [2] and +2.5 ppm/yr in 2021 [3]). Despite political efforts to reduce CO_2 emissions – for example with the Paris agreement [4] – fossil CO_2 emissions in 2022 are estimated to be higher than ever before in the industrial era [3]. It was shown by integrated assessment modeling that massive enlargement of carbon capture capacity is required to still reach the aims of the Paris agreement that limit global warming to 1.5 °C above pre-industrial levels [5]. Additionally, there are large R&D efforts for Power-to-X technologies converting (excess) renewable energy into heat, other forms of energy or valuable chemicals [6]. Plasma conversion technology offers a unique solution for utilization of captured carbon dioxide by converting it into the value-added chemical carbon monoxide (CO) which is an important reactant in chemical industry as part of many carbonylation reactions or as a component of synthesis gas (mixture of CO and H_2).

The dissociation of carbon dioxide is represented by the following endothermic reaction:

$$CO_2 \rightarrow CO + \frac{1}{2}O_2 \tag{1}$$

for which a reaction enthalpy of $\Delta H = 2.93$ eV/molecule is required.

Several plasma sources have been investigated in the past few years for CO_2 dissociation [7], including microwave (MW) plasmas [8–15], dielectric barrier discharges [16,17], radio-frequency plasmas [18], thermal arc discharges [19–21] and gliding arc discharges [22,23]. Besides gliding arc plasmas, especially microwave plasma torches were shown to yield high energy efficiency and high CO_2 conversion [7]. In a microwave plasma torch, the plasma is known to exhibit two distinct modes depending mainly on pressure (and slightly on microwave power) [12,24,25]: For pressures below about 150 mbar, the plasma is diffuse, spreading over the full radius of the reactor quartz tube. At pressures above about 150 mbar, the plasma is in the contracted mode, being drawn together to a narrow filament in the center of the reactor tube. Highest plasma energy efficiencies are reported for pressures around 150 mbar, i.e. close to the transition from the diffuse to the contracted regime [12]. Towards higher pressures, plasma energy efficiency typically declines, reaching the lowest value at atmospheric pressure, which is the most relevant pressure for industrial application. Especially at high specific energy input (SEI), i.e. large microwave power and/or small feed gas flow rate, energy efficiency heavily drops

* Corresponding author.
E-mail address: christian.kiefer@ipp.mpg.de (C.K. Kiefer).

https://doi.org/10.1016/j.cej.2023.148326
Received 18 September 2023; Received in revised form 8 December 2023; Accepted 22 December 2023
Available online 27 December 2023

when the pressure is raised from sub-atmospheric pressures of 150–200 mbar towards atmospheric pressure. This can be explained as follows: In the contracted regime, vibrational, rotational and translational degrees of freedom are in equilibrium at a temperature of around $T \approx 6000$ K [24,26]. Thus, CO_2 dissociation is achieved via thermal CO_2 splitting which theoretically allows for energy efficiencies up to around 50% [7,27]. However, reverse reactions of carbon monoxide with oxygen back to CO_2 occurring especially at high SEI and high pressure lead to considerably lower energy efficiency.

As indicated in the discussion above, the performance of a plasma process for the decomposition of CO_2 into carbon monoxide and oxygen is commonly characterized by two figures of merit: conversion and energy efficiency. Many attempts are reported to improve the performance of microwave plasmas close to atmospheric pressure: L. F. Spencer and A. D. Gallimore [8] inserted a Rh/TiO_2 catalyst in the effluent of an atmospheric pressure surfaguide discharge which, however, even decreased energy efficiency due to an enhancement of recombination reactions of CO with oxygen to produce CO_2. The usage of supersonic expansion of the plasma into the reactor tube by employing a nozzle at its bottom limited the energy efficiency to a maximum value of 15% [9]. An improvement in energy efficiency from below 15% obtained with continuous wave to 27% is obtained in a coaxial torch by pulsing the microwave power with a pulse time of $t_{on} = 2$ µs, which is explained to be the result of a modulation of temperatures across the pulse [10]. Most successful attempts to improve energy efficiency close to atmospheric pressure have been obtained by quenching the effluent of a microwave plasma torch, i.e. rapidly reducing the gas temperature to suppress recombination reactions of carbon monoxide and oxygen. Using a nozzle in the effluent, conversion at 4.7 slm could be enhanced from 5% (when no nozzle was installed) to 35% (when a nozzle with 2.5 mm diameter is used) [13]. Exceptionally high energy efficiencies and conversions have been obtained in a setup in which the gas is injected in reverse vortex configuration and leaves the resonator through a set of water-cooled quenching channels, allowing for conversions up to 57% and energy efficiencies up to 30% [15].

The investigations summarized above have in common that they were all performed using laboratory-scale plasma reactors and energy efficiencies which are reported in the afore cited publications consider only the power that is absorbed by the plasma P_{abs}, but not the total active electrical power that is required by the full system $P_{active,tot}$. However, assessing the techno-economic feasibility of plasma-based CO_2 dissociation on industrial scale requires to know the overall power consumption for carbon monoxide production. For CO_2 dissociation via microwave plasmas, this involves the power consumption of the microwave sources, vacuum pumps, product gas separation and other peripheral equipment.

In the following, the power requirements of a plasma torch setup are investigated that is still on the laboratory scale (forward microwave powers up to 3 kW), thus also not yet optimized for industrial application. However, it will be strictly distinguished between the plasma energy efficiency η_p and the wall-plug energy efficiency (or total energy efficiency) η_{tot}. The plasma energy efficiency η_p considering only the power absorbed by the plasma P_{abs} will be utilized to get deeper insight into the physics and the chemical reactions happening in the CO_2-dissociating plasma. Wall-plug energy efficiency η_{tot} considering the total electrical power consumption $P_{active,tot}$ will be used to assess the suitability of the plasma-based CO_2 splitting for industrial application. Sections 3 and 4 will compare different configurations of a microwave plasma torch with respect to η_p and η_{tot}.

Suitability for industrial application requires also a stable system that can reproducibly be operated over long durations. Furthermore, to be considered as a Power-to-X technology, it must be compatible with the electric power supply of the future which is anticipated to be dominated by solar and wind power, both exhibiting large temporal fluctuations in the provided electricity. These aspects are examined for the microwave plasma torch in Section 5. Finally, industrial CO_2 streams might – depending on their source – contain significant amounts of impurities. In Section 6, the impact of some impurities (nitrogen, oxygen, argon, air and synthetic air) in the feed gas stream on conversion and energy efficiency is systematically investigated.

2. Experimental setup

This section describes the general experimental setup. Details specific to the experiments described in Sections 3–6 are described in the respective sections. The center of the experimental setup (see Fig. 1) is a microwave plasma torch powered by a microwave generator running at a frequency of 2.45 GHz. This microwave plasma torch consists of a combination of a cylindrical resonator and a coaxial resonator, thus allowing for two different modes [28]. In the coaxial mode, the electric field is highest at the tip of the inner conductor of the coaxial resonator. This electric field enhancement at the top of the brass pin helps to ignite the plasma. In the cylindrical TE_{10} mode, electric field is highest in the middle of the cylindrical resonator. This mode is utilized to continuously sustain the plasma after ignition. A quartz tube (inner diameter: 26 mm, outer diameter: 30 mm) in the center of the resonator confines the plasma gas and acts as the reaction chamber [29].

The microwaves that are fed into the plasma torch are generated by a magnetron (magnetron head MH3000S-213BB with power supply ML3000D-111TC, both from Muegge) which can provide a maximum forward microwave power of 3 kW. A system of rectangular waveguides (WR340) directs the microwaves towards the resonator. This system includes a protection window made of Teflon and a manual 3-stub tuner being used for impedance matching to minimize the microwave power that is reflected back from the plasma.

Gas is injected through tangential gas inlets to create a swirl flow. As a result, the hot plasma gas in the center is surrounded by an envelope of cold gas protecting the quartz glass from melting. Flow rates up to around 200 slm are achievable (the unit slm being a "standard liter per minute", defined here with respect to a standard pressure of 1013 hPa and a standard temperature of 0 °C). After exiting the plasma torch, the hot effluent gas passes through a 2 m double-pipe heat exchanger lowering the gas temperature down to room temperature. This is necessary to protect the vacuum pump from any damage and ensures having a well-equilibrated gas at the position where its composition is measured.

At the end of the heat exchanger, the gas composition is measured by means of mass spectrometry (see [30] for details). Knowing the relative molar flow rates of the different gases in the effluent of the plasma torch, the CO_2 conversion χ can be determined which is defined as follows:

$$\chi := \frac{\dot{n}_{CO2,in} - \dot{n}_{CO2,out}}{\dot{n}_{CO2,in}} = 1 - \frac{\dot{n}_{CO2,out}}{\dot{n}_{CO2,in}}. \quad (2)$$

In this equation, $\dot{n}_{CO2,in}$ and $\dot{n}_{CO2,out}$ denote the molar flowrates of CO_2 in the inflow and the outflow of the reactor, respectively.

At the end of the heat exchanger, a 3-way ball valve (120VKD025-L from Pfeiffer Vacuum) allows to direct the gas stream directly to the exhaust chimney or, alternatively, to suck out the gas stream by a rotary vane vacuum pump (TRIVAC® D 16 B Ex from Leybold). While the first option ensures operation at atmospheric pressure, the latter option allows to control the pressure over a wide range from atmospheric pressure down to below 100 mbar by using a diaphragm valve. Throughout this manuscript, data presented for "atmospheric" pressure always refer to experiments in which the gas stream flows directly to the exhaust chimney, i.e. the pressure in the effluent is atmospheric (in case there is a constriction between resonator end effluent like e.g. a nozzle, the pressure in the resonator might even be somewhat above atmospheric pressure). "900 mbar" refers to a pressure in the resonator being held as close as possible to 900 mbar by adjusting the diaphragm valve.

Experiments were performed in three different configurations of the plasma torch (see Fig. 2). In the standard configuration, gas is injected

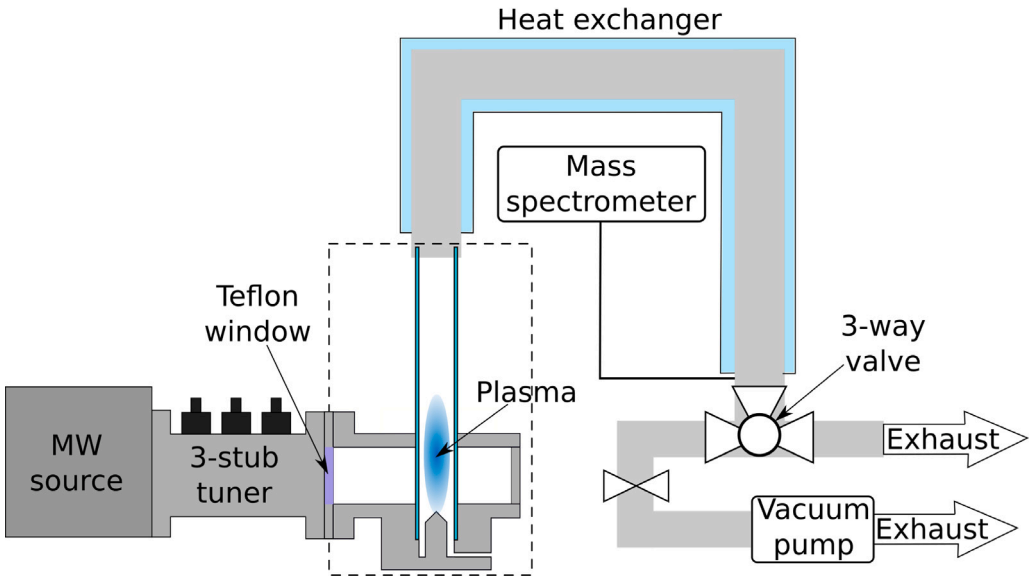

Fig. 1. Experimental setup. The plasma torch itself is surrounded by a dashed rectangle. Different configurations of the plasma torch are shown in Fig. 2.

Table 1
Overview of the configurations used in the different figures.

Figure	Standard	Nozzle	Cooling channels & reverse vortex
Fig. 5	x	x	x
Fig. 6		x	x
Fig. 8	x	x	x
Fig. 9	x		
Fig. 10			x
Fig. 11			x
Fig. 12	x	x	
Fig. 13			x
Fig. 14	x		x
Fig. 15			x
Fig. 17	x		
Fig. 18	x		
Fig. 19		x	

through four tangential gas inlets at the bottom of the reactor and swirls upwards inside a quartz tube of length 16 cm (also different lengths could be used). An extensive investigation of the standard configuration can be found in [12]. In the nozzle configuration, a water-cooled copper nozzle is attached above the 84 mm long quartz tube. Three different diameters for the nozzle were tested: 10 mm, 5 mm and 2.5 mm. A picture of the 10 mm-diameter nozzle is provided as a supplementary file. More details on CO_2 conversion with the nozzle configuration can be found in [13]. In the configuration with the cooling channels, gas is injected through tangential gas inlets (diameter: 1.5 mm) at the top of the resonator to induce a reverse vortex flow configuration. After passing through the active plasma zone, the effluent passes through a water-cooled copper piece comprising of a constriction of 5 mm diameter that splits up into four gas channels of 4 mm diameter to enlarge the cooling surface [15]. Also this copper piece sits atop of a 84 mm long quartz tube. Table 1 shows where in this manuscript which configuration was deployed.

2.1. Electrical power measurement

To determine the electrical power required for the conversion of CO_2, an energy metering system was set up which is used to measure the electrical power consumption of the microwave source and of the vacuum pump individually. Fig. 3 shows the circuit diagram of the power metering system which is based on two Energy Meter 525–230 from Weidmüller GmbH & Co. KG, one for monitoring the power consumption of the microwave source and one for the vacuum pump. For both, the microwave power supply as well as the vacuum pump, all three phases (L1, L2, L3) of the three-phase alternating current are monitored. Voltages are measured parallel to the phases and currents are measured via inductive current transformers (CMA-CTM-7-32-1A-0.2VA-1 from Weidmüller). The data of the energy meters is read out on a PC using the software ecoExplorer Go®.

Using this energy metering system, the active power P_{active}, the reactive power $P_{reactive}$, the apparent power and the power factors can be measured for each of the six phases and thus, also for each device and the entire electrical system. The most important quantity throughout this study is the active electrical power P_{active} since this is the power that is actually used up by the system and thus is the major determinant of its operational expenditure (OPEX). Summing up the active power consumptions of the vacuum pump and the microwave power supply yields the total active power:

$$P_{active,tot} = P_{active,VP} + P_{active,MW}. \quad (3)$$

Other electrical devices such as a chiller to provide cooling water and small devices such as pressure gauges and mass flow controllers are neglected throughout this study. The chiller was neglected since it is expected that in an industrial process, one would use dwell water instead of a chiller to provide cooling water. Small devices are neglected since they only consume power on the order of W whereas the plasma torch itself and the vacuum pump consume power of the order of kW.

During the experiments, the electrical power was measured at least for 2 min, usually even for more than 5 min. Fig. 4 shows a typical time trace for the active power measurement depicting the deviations of P_{active} from its mean value. For both, the vacuum pump and the microwave power supply, one observes only small fluctuations below 10 W apart from its mean value. Taking into account not only these small fluctuations in the power consumption, but also errors due to fluctuations in the grid and the error for active power measurement of the energy meters themselves (class 1), one obtains a very conservative value for the total error of 1.4%. Assuming that all errors are stochastically independent, the total error is even as small as 1.1%.

3. Plasma energy efficiency

In this section, the energy demands of only the plasma sub-system carrying out the CO_2 dissociation will be considered. The performance for the plasma sub-system is characterized by two figures of merit: the

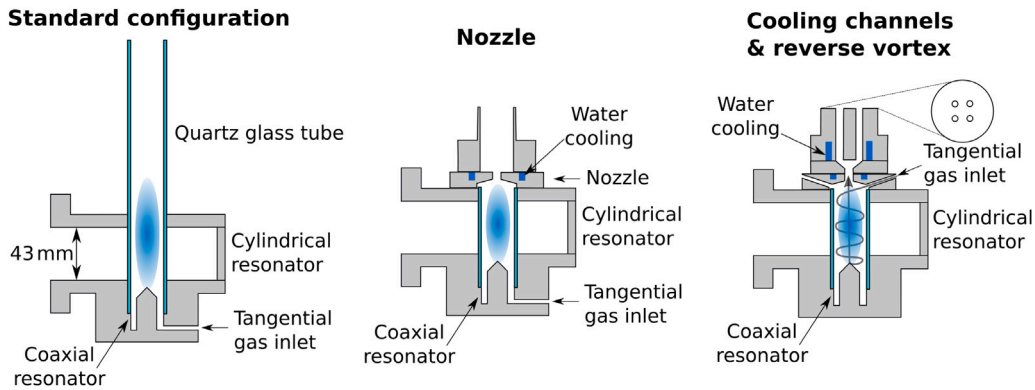

Fig. 2. The three different configurations of the plasma torch: Standard configuration, nozzle configuration and cooling channels & reverse vortex.

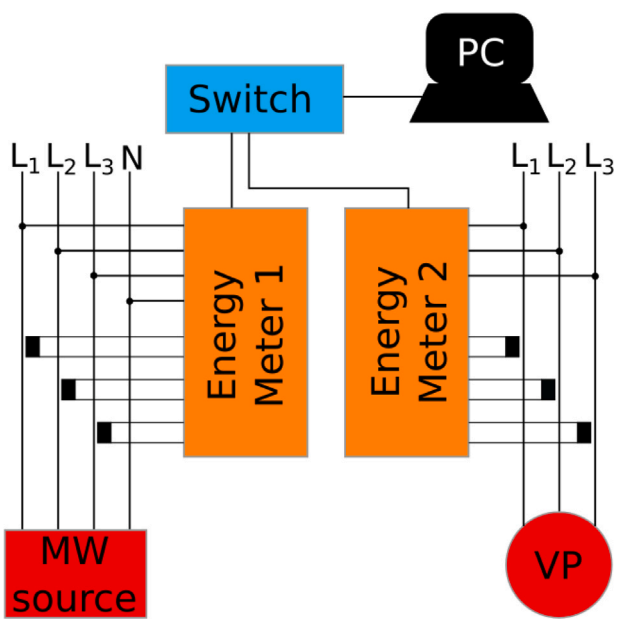

Fig. 3. Setup of the energy metering system to measure the power consumption of the microwave (MW) source and the vacuum pump (VP).

conversion χ and the plasma energy efficiency η_p. Both yield valuable insights into the physics and the reaction chemistry of thermal CO_2 dissociation in the three different configurations of the plasma torch. Based on the specific energy input

$$\mathrm{SEI_p} := \frac{P_{\mathrm{abs}}}{\tilde{\Gamma}_{\mathrm{CO2,in}}}, \tag{4}$$

the plasma energy efficiency is defined as

$$\eta_p := \chi \cdot \frac{\Delta H}{\mathrm{SEI_p}} = \chi \cdot \frac{\Delta H \cdot \tilde{\Gamma}_{\mathrm{CO2,in}}}{P_{\mathrm{abs}}}. \tag{5}$$

In the above equations, ΔH is the reaction enthalpy required for reaction (1), $\tilde{\Gamma}_{\mathrm{CO2,in}}$ the particle inflow rate of CO_2 and P_{abs} the microwave power that is absorbed by the plasma. The absorbed power $P_{\mathrm{abs}} = P_{\mathrm{in}} - P_{\mathrm{ref}}$ is calculated from the incident microwave power P_{in} and the reflected microwave power P_{ref}.

The database examined in this section and Section 4 consists of power scans (with absorbed powers in the range of 600 W up to 2700 W) for the following flows and configurations:

- In standard configuration, experiments were performed at 150 mbar, 200 mbar, 900 mbar and atmospheric pressure, each at 9.3 slm and 14.0 slm.
- For 9.3 slm and 14.0 slm, the following conditions were investigated: 10 mm-nozzle at atmospheric pressure and 5 mm-nozzle as well as 2.5 mm-nozzle at 900 mbar and atmospheric pressure.
- The cooling channels setup at atmospheric pressure (for 9.3 slm and 14.0 slm) and at 900 mbar (for 3.7 slm, 4.7 slm, 9.3 slm, 14.0 slm and 18.6 slm).

Conversions and plasma energy efficiencies for these experiments are shown in Fig. 5. It was already pointed out in [12] that at a given pressure, the major determinant of χ and η_p is the specific energy input summarizing the effects of the absorbed power and the CO_2 flow rate. For a given $\mathrm{SEI_p}$, highest energy efficiencies are achieved in standard configuration at sub-atmospheric pressure operation at pressures around 150 mbar where the transition from a diffuse plasma to a contracted plasma takes place. At low pressures, conversion increases approximately linearly with $\mathrm{SEI_p}$ and thus, η_p is almost constant across different specific energy inputs.

At higher pressures (here: 900 mbar or atmospheric pressure) in the standard configuration, conversion tends to saturate and eventually even falls off when increasing $\mathrm{SEI_p}$. As can be seen from Fig. 5(a) conversions at 900 mbar and atmospheric pressure are limited to values well below 20%. This also results in heavily decreasing η_p upon increasing the specific energy input. Such a reduced performance at higher pressures and high $\mathrm{SEI_p}$ can be explained by the quenching rates $|{}^{dT}/_{dt}|$ of the plasma effluent being smaller under these conditions than at around 150 mbar or lower $\mathrm{SEI_p}$, leaving enough time for recombination reactions between carbon monoxide and oxygen. These recombination reactions resulting in losses of CO and thus, reduced conversion, are mainly [14]

$$CO + O + M \rightarrow CO_2 + M, \tag{6}$$

but also

$$CO + O_2 \rightarrow CO_2 + O. \tag{7}$$

Rapid quenching (with quenching rates $\geq 10^7$ K/s for ideal quenching [31]) is required to minimize the recombination reactions.

The standard configuration is characterized by the absence of any additional element being dedicated to quench the effluent of the plasma. Thus, quenching occurs exclusively via convection and diffusion in this configuration. It was demonstrated via CFD modeling that immediately downstream of the plasma, strong cooling occurs [14]. This cooling is mainly convective cooling as it is considerably stronger than conductive cooling. Since convective cooling increases with increasing flow and $\mathrm{SEI_p} \propto \tilde{\Gamma}^{-1}_{\mathrm{CO2,in}}$, highest quenching rates are expected at low specific energy input at a given power. Moreover, one can expect stronger quenching also at lower absorbed power P_{abs} (at given $\tilde{\Gamma}_{\mathrm{CO2,in}}$) as an increase in the absorbed power increases the volume of the plasma [12], thus reducing the volume of cold gas that brings about the convective cooling. As a result, highest plasma energy efficiency in the standard configuration is observed in general for low $\mathrm{SEI_p}$.

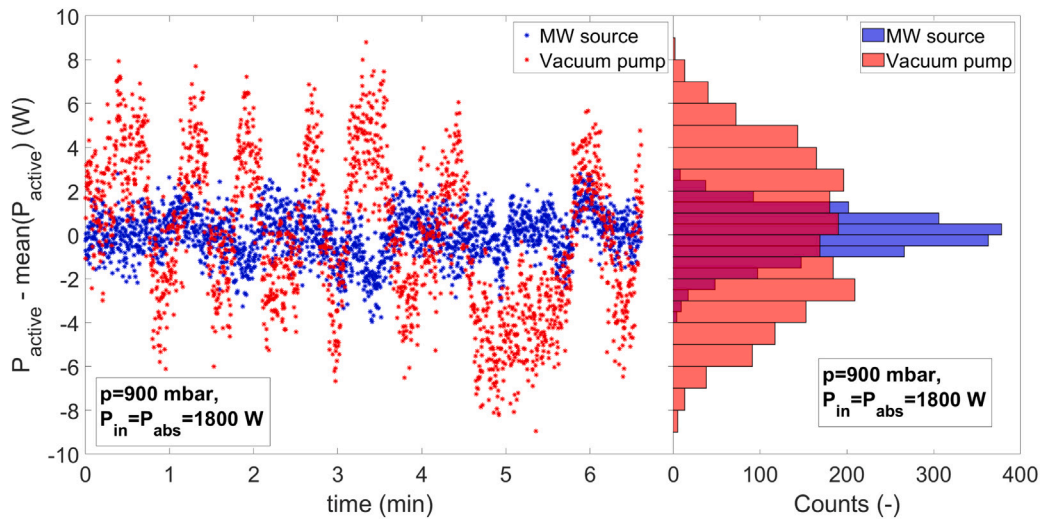

Fig. 4. Time traces of deviations of the active power measurement from their mean value, and corresponding histograms.

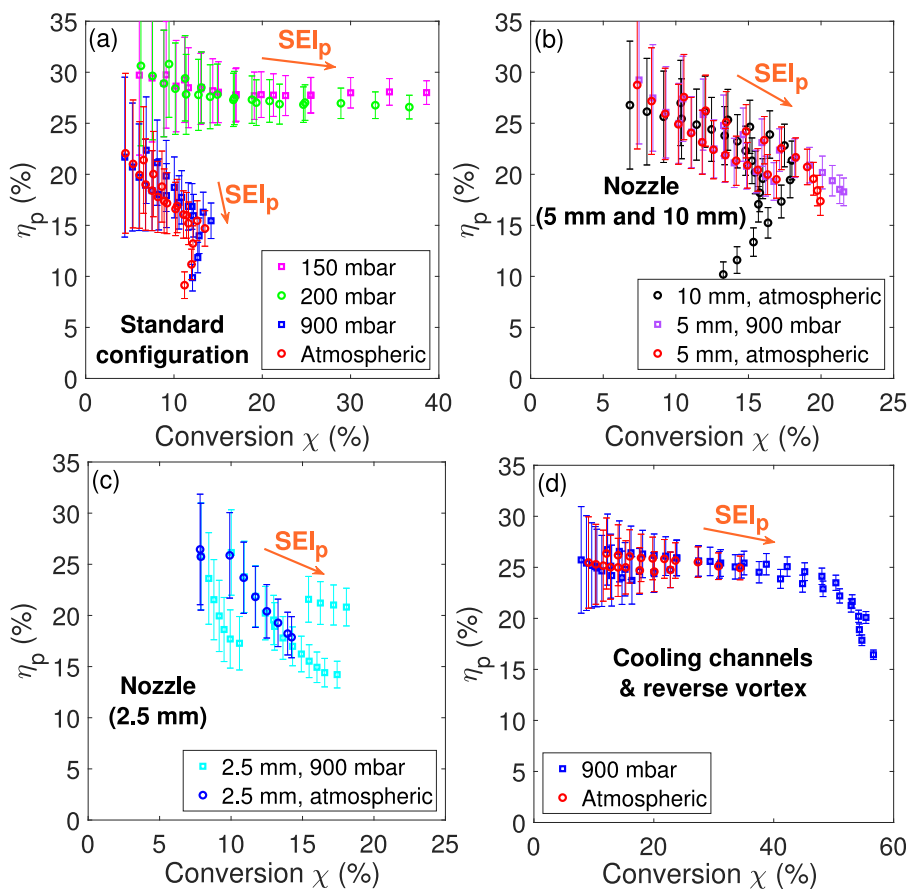

Fig. 5. Plasma energy efficiency η_p versus conversion χ for all configurations examined throughout this paper. The orange arrows give the direction in which the specific energy input is increased.

A detailed analysis of the nozzle configuration and its benefits on the CO_2 conversion is given in [13,14]. For the range of flow rates (9.3 slm to 14.0 slm) investigated in this paper, the best performance could be achieved with the 5 mm-nozzle (see Fig. 5(b)). For this diameter, plasma energy efficiencies up to $(29 \pm 7)\%$ (at a flow rate of 14.0 slm) and conversions up to $(21.6 \pm 1.6)\%$ (at a flow rate of 9.3 slm) could be achieved at 900 mbar. This improvement close to atmospheric pressure compared to the standard configuration can be explained by the improved quenching of the plasma effluent. It is caused by forcing the hotter gas in the center of the reactor to mix with the colder gas in the outer layers of the reactor and by bringing the hot gas into contact with the water-cooled surfaces of the nozzle [13,14]. For the 2.5 mm-nozzle (Fig. 5(c)), an additional effect can come into play: Due to the small nozzle diameter, a pressure difference Δp between resonator and effluent can build up, especially for high feed flow rates and high power input. If the ratio between the pressure in the resonator and effluent pressure is high enough, supersonic expansion of the effluent after passing through the nozzle will additionally enhance the quenching.

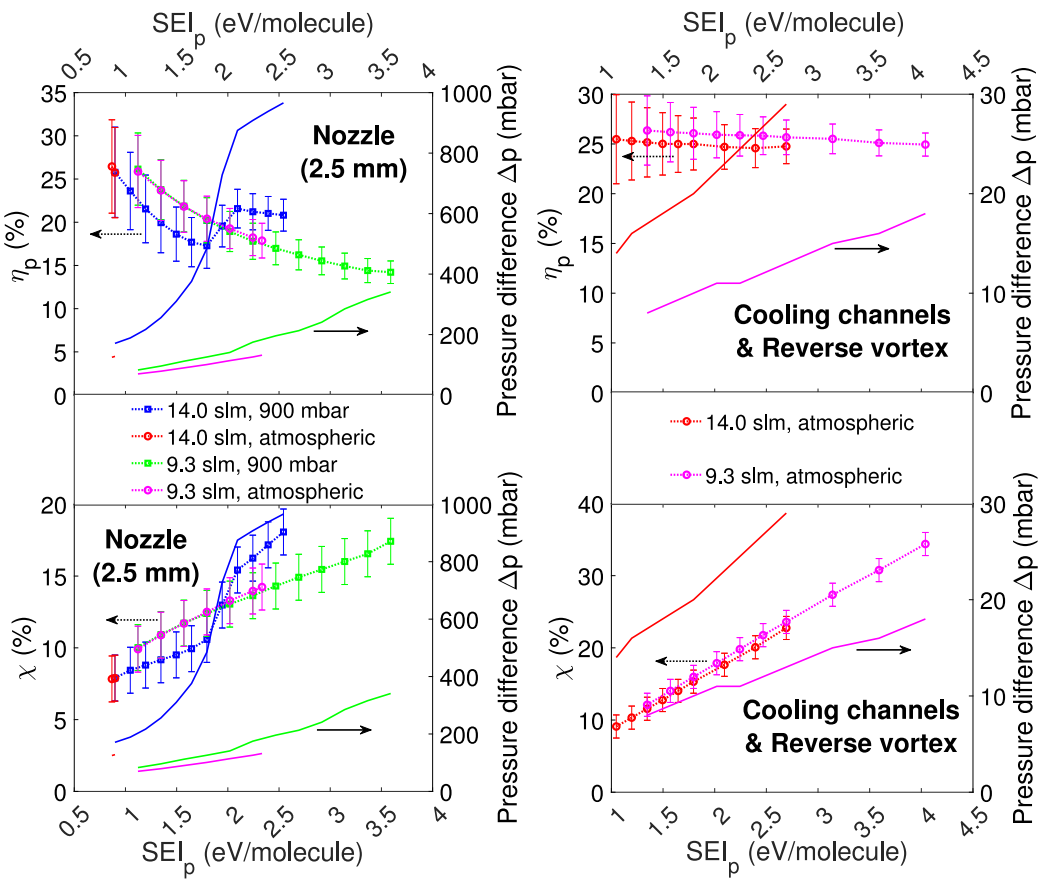

Fig. 6. Plasma energy efficiency (top) and conversion (bottom) as a function of specific energy input for the 2.5 mm-nozzle and the cooling channels configuration (dotted lines). The solid lines give the pressure difference between resonator and effluent Δp.

This can be seen in Fig. 6 for a flow rate of 14.0 slm where at $SEI_p \approx 2$ eV/molecule the pressure difference starts to exceed around 500 mbar, and a jump upwards in conversion and plasma energy efficiency occurs. For 9.3 slm, the pressure drop Δp remains below 400 mbar and thus no sudden increase in χ and η_p is observed.

Such a pressure drop also has the disadvantage that a force is required to push the gas through the nozzle. Theoretically, this results in an additional power requirement of $P = (\text{volumetric flow}) \cdot \Delta p$ for the CO_2 conversion process. Practically, the additional power requirement is given by the electrical power consumption of the vacuum pump needed to establish this pressure drop ($P_{\text{active,VP}}$ around 500 W as shown in Section 4). For the calculation of a total energy efficiency, this power requirement needs to be considered as well. Furthermore, a vacuum pump requires maintenance which will add upon the operational costs.

The configuration of the plasma torch with the cooling channels and the reverse vortex was already analyzed in detail by A. Hecimovic et al. [15]. It relies on two effects that can be disentangled from each other. On the one hand, high quenching rates allow to push conversion and plasma energy efficiency close to atmospheric pressure towards high values that in standard configuration, would only be obtained at sub-atmospheric pressure operation (see Fig. 5). This enhanced quenching is achieved by the convective cooling mediated by the gas-surface interaction in the water-cooled effluent channels. Splitting up the one gas channel into four channels increases the effective cooling surface and might even induce some turbulence, both being desired effects that considerably improve the quenching of the plasma effluent. On the other hand, high stability of the plasma is achieved by the combination of the reverse vortex flow with the narrow gas inlets (only 1.5 mm in diameter). This allows operation at very high specific energy inputs. Both effects together, i.e. improved stability of the plasma and rapid quenching, allows to reach very high conversions up to (56.6 ± 1.6)% (obtained at a flow of 3.7 slm and an absorbed power of 2700 W, corresponding to $SEI_p = 10.1$ eV/molecule).

It was demonstrated in [15] and one can see in Fig. 5 that experiments performed at 900 mbar in the cooling channels configuration yield identical performance in terms of χ and η_p as in atmospheric pressure operation, i.e. with vacuum pump being disconnected. This is related to the pressure drop being comparably small (as can be seen in Fig. 6, $\Delta p < 20$ mbar at 9.3 slm and $\Delta p < 30$ mbar at 14.0 slm). The possibility to remove the vacuum pump from the experimental setup while maintaining high χ and η_p is an important conclusion for industrial applicability since removing the vacuum pump leads to a reduction of capital expenditure as well as operational expenditure (in particular by deducting $P_{\text{active,VP}}$ from the power requirements). On the other hand, even if for operation of the facility, no vacuum pump is required, it might still be required for igniting the plasma since ignition is facilitated by low pressures. This is for example done in the experiments described in Section 5 where the vacuum pump was employed for ignition, but is disconnected afterwards.

It is known from literature [8,9] that there is usually a trade-off between conversion and plasma energy efficiency for CO_2 dissociation via microwave plasmas. Such a trade-off between χ and η_p is observed also for all three configurations of the plasma torch. For the cooling channels configuration, for example, highest conversion of $\chi = (56.6 \pm 1.6)\%$ is achieved at a plasma energy efficiency of only $\eta_p = (16.4 \pm 0.5)\%$ whereas highest plasma energy efficiency of $\eta_p = (27 \pm 4)\%$ is reached for a comparably rather low conversion of $\chi = (12.3 \pm 1.6)\%$. In the following section, it will be shown that this trade-off exists only when plasma energy efficiency is considered versus conversion and the picture looks different when considering wall-plug energy efficiency instead of plasma energy efficiency.

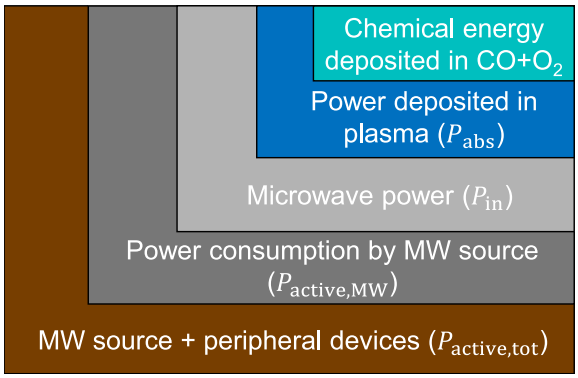

Fig. 7. Schematic visualization of the power distribution within the system.

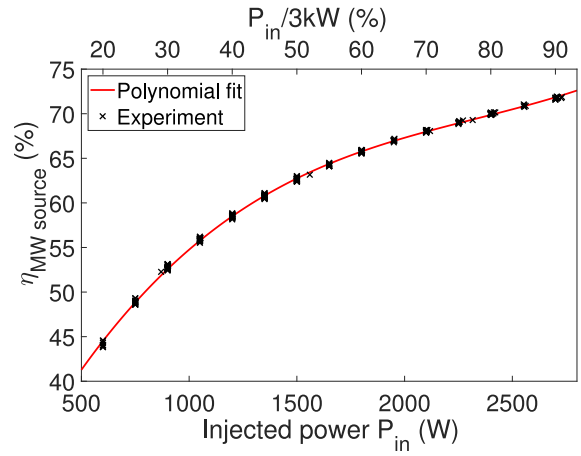

Fig. 8. Energy efficiency of the microwave source as a function of forward microwave power. The red line is a polynomial fit for guiding the eye.

4. Wall-plug energy efficiency

To assess the economic viability of plasma-based CO_2 dissociation, it is not sufficient to consider the energy efficiency of the plasma sub-system alone η_p. Fig. 7 visualizes the different contributions to the total electrical power consumption $P_{\text{active,tot}}$ of the entire system that must be considered. Besides the power losses of the plasma sub-system, also power losses in the form of reflected microwave power $P_{\text{ref}} = P_{\text{in}} - P_{\text{abs}}$ have to be taken into account. This can be described by defining an energy efficiency for the coupling of the injected microwaves to the plasma:

$$\eta_{\text{MW coupling}} := \frac{P_{\text{abs}}}{P_{\text{in}}}. \tag{8}$$

Microwaves can be generated either by a magnetron or by a solid-state power generator. Whatever technique is used, one can expect a certain inefficiency in converting the electrical power to microwave power. This is described by an energy efficiency of the MW source considering the generated forward microwave power P_{in} with respect to the active electrical power consumed by the microwave source $P_{\text{active,MW}}$:

$$\eta_{\text{MW source}} := \frac{P_{\text{in}}}{P_{\text{active,MW}}}. \tag{9}$$

In addition to the microwave source, also other electricity-consuming peripheral devices are required for the process. In our case, the dominant peripheral device is the vacuum pump required for sub-atmospheric pressure operation. The requirement for additional electricity-consuming peripheral equipment can be expressed as an energy efficiency as well:

$$\eta_{\text{equipment}} := \frac{P_{\text{active,MW}}}{P_{\text{active,tot}}}. \tag{10}$$

Considering the above discussion, the wall-plug energy efficiency (or total energy efficiency) is defined with respect to the total active electrical power consumed by the entire system $P_{\text{active,tot}}$ as follows:

$$\eta_{\text{tot}} := \chi \cdot \frac{\Delta H \cdot \tilde{\Gamma}_{\text{CO2,in}}}{P_{\text{active,tot}}} = \eta_{\text{p}} \cdot \eta_{\text{MW coupling}} \cdot \eta_{\text{MW source}} \cdot \eta_{\text{equipment}}. \tag{11}$$

As can be seen from this equation, the wall-plug efficiency can be written as the product of four energy efficiencies. Besides the plasma energy efficiency, especially the energy efficiency of the microwave source $\eta_{\text{MW source}}$ will be shown in the following sections to be a major determinant of η_{tot}. The term "wall-plug energy efficiency" was chosen here for η_{tot} since it describes the energy efficiency in the conversion of electricity (drawn from the wall-plug) to the final product (CO molecules), accounting for all intermediate steps in which energy is converted into another form.

In electrolysis literature, the performance of different electrolyzers is often described on the basis of the electric power consumption EPC which gives electrical energy (in kWh) that is needed to produce one cubic meter of CO (N m^3 defined at 0°C and 1013 hPa), but without taking peripheral equipment into account [32]. In the framework of this paper, the EPC will be generalized and the electric power consumption will be defined as follows:

$$\text{EPC} := \frac{P_{\text{active,tot}}}{\Gamma_{\text{CO,out}}} = \frac{\Delta H \cdot N_{\text{A}}}{V_m \cdot \eta_{\text{tot}}}. \tag{12}$$

In this equation, $\Gamma_{\text{CO,out}} = \chi \cdot \Gamma_{\text{CO2,in}}$ denotes the flow rate of carbon monoxide in the outflow, N_{A} the Avogadro constant and $V_m = 22.414 \cdot 10^{-3}\ \text{m}^3/\text{mol}$ the molar volume. The EPC as defined in Eq. (12) has the advantage that it can be applied to plasma systems as well as CO_2 electrolysis systems and other CO_2 dissociation technologies.

4.1. Microwave source

Fig. 8 gives the energy efficiency $\eta_{\text{MW source}}$ of the microwave source used throughout this study, consisting of the magnetron head and the microwave power supply, as a function of the forward microwave power P_{in}. It is measured during the plasma experiments described in Section 3. The nominal power of the magnetron is 3 kW. When the microwave power is increased towards this maximum output power, energy efficiency of the microwave source increases. At $P_{\text{in}} = 2.7$ kW, an energy efficiency of 72% is reached.

It shall be noted here that for 915 MHz magnetrons, one can expect even slightly higher energy efficiencies. At University of Stuttgart, a plasma torch similar to the one used throughout this study, but at a microwave frequency of 915 MHz, was already developed. This plasma torch was demonstrated to exhibit similar plasma characteristics as the 2.45 GHz plasma torch (e.g. the gas temperatures of a humidified air plasma were measured to be similar in both devices) [28]. It was demonstrated by W. Bongers et al. [9] that at a given specific energy input, similar plasma energy efficiencies can be achieved in both plasma torches. However, the plasma volume of the 915 MHz plasma torch is about 20 times larger than the plasma volume in the 2.45 GHz plasma torch [33]. Thus, the 915 MHz plasma torch presents a convenient way to upscale the CO_2 dissociation process while potentially achieving even higher $\eta_{\text{MW source}}$ and thus, higher wall-plug energy efficiencies.

4.2. Vacuum pump

The electrical power consumption of the vacuum pump was measured in an experiment in standard configuration with pure CO_2 flow (i.e. no plasma). The pressure in the reactor is controlled by means of the diaphragm valve placed in the gas lines in front of the vacuum

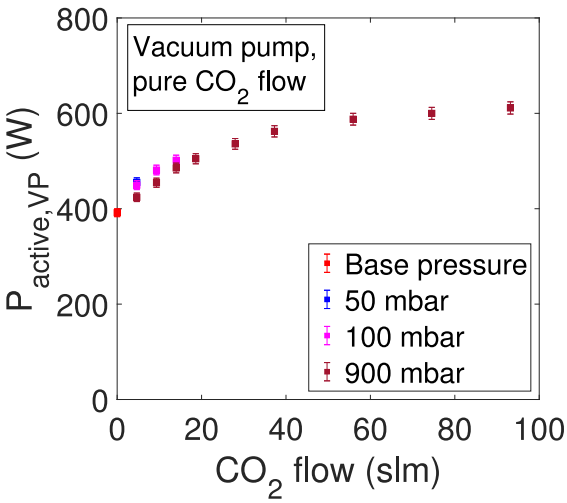

Fig. 9. Active electrical power consumption of the vacuum pump.

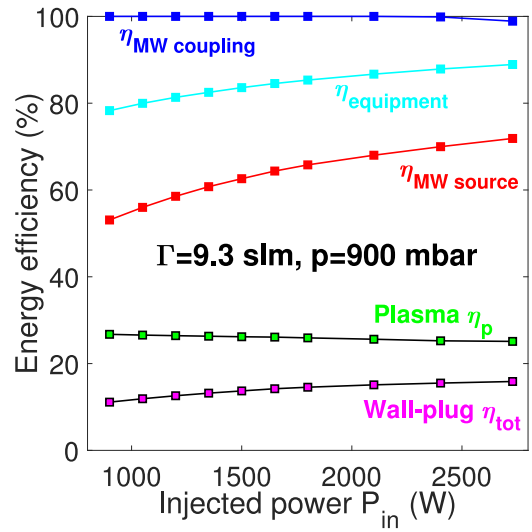

Fig. 10. Overview over the different energy efficiencies involved in Eq. (11) for an experiment performed in the configuration with cooling channels and reverse vortex.

pump (see Fig. 1). Results for the active power consumption of the vacuum pump are shown in Fig. 9. One observes that the active power consumption of the vacuum pump is fairly independent of the pressure in the reactor, but increases with increasing flow from around 400 W at no flow to around 600 W at 100 slm. Additionally, the vacuum pump requires a reactive power of $P_{\text{reactive,VP}} = 1$ kVAr which in countries with reactive power pricing might lead to additional operational costs [34,35].

Since the dissociation of CO_2 according to Eq. (1) leads to a volume increase by a factor of $(1 + \chi/2)$, the power consumption of the vacuum pump during plasma experiments can be slightly different from the one for pure CO_2 reported in Fig. 9. Additionally, the power consumption might also depend on the type of molecule that is pumped. Thus, for results reported in Section 4.3, the power requirements for the vacuum pump were measured during every experiment individually.

4.3. Full system

The wall-plug energy efficiency is determined by monitoring the electrical power consumption of the microwave power supply and the vacuum pump in parallel to the mass spectrometry measurements. Fig. 10 shows the resulting energy efficiencies obtained for an experiment employing the cooling channels & reverse vortex configuration. In this experiment, one observes a slight decrease in plasma energy efficiency η_p from $(27 \pm 4)\%$ down to $(25.1 \pm 1.2)\%$ when the injected power is raised from 900 W to 2730 W. Interestingly, the wall-plug energy efficiency shows the opposite trend and even increases from 11.1% to 15.9% in the same range for P_{in}. This is explained by the influence of $\eta_{\text{MW source}}$ on the total energy efficiency that increases with increasing power. Also $\eta_{\text{equipment}}$ appears to increase, thus pushing up the wall-plug energy efficiency towards higher powers. $\eta_{\text{MW coupling}}$ is always close to 100%, demonstrating that there are almost no power losses due to reflection of microwaves by the plasma. Note that among all four energy efficiencies (η_p, $\eta_{\text{MW coupling}}$, $\eta_{\text{MW source}}$, $\eta_{\text{equipment}}$) contributing to the wall-plug energy efficiency, the one of the plasma sub-system is by far the lowest. Thus, employing a plasma that can efficiently dissociate CO_2 is key of achieving high total energy efficiencies.

Fig. 11 shows the results for η_{tot} and χ obtained with the cooling channels configuration. Interestingly, there is no general trade-off between conversion and total energy efficiency η_{tot} and only at very high conversion (high SEI_p), increasing further the conversion results in a decrease in total energy efficiency. Instead, for the given microwave source, one observes a maximum in total energy efficiency for conversions between 30% and 40%. For CO_2 feed flow rates $\geq$ 9 slm,

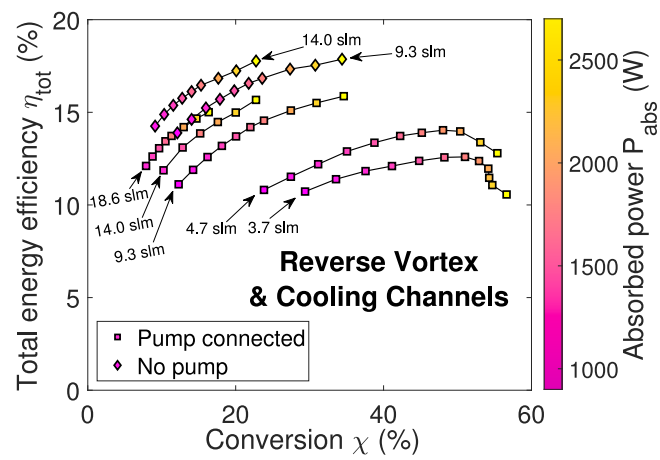

Fig. 11. Wall-plug energy efficiency for the cooling channels setup. At 900 mbar (pump connected), data for 3.7, 4.7, 9.3, 14.0 and 18.6 slm is shown and atmospheric pressure (pump disconnected) data for 9.3 slm and 14.0 slm.

increasing the microwave power increases conversion and wall-plug energy efficiency simultaneously. For high CO_2 feed flow rates, the best wall-plug energy efficiency is achieved at the highest microwave power where also $\eta_{\text{MW source}}$ is highest. The highest total energy efficiency achieved for the cooling channels configuration is $\eta_{\text{tot}} = 17.9\%$ for a conversion of $\chi = (34.4 \pm 1.6)\%$. It is important to note the clear enhancement in total energy efficiency by about 2% when the vacuum pump is disconnected from the system.

One can also see the positive effect of disconnecting the vacuum pump when comparing the 900 mbar data with data from atmospheric pressure experiments for the standard configuration and the 5 mm-nozzle (see Fig. 12): Plasma energy efficiency η_p is almost not affected by removing the pump while the electrical power requirement decreases by $P_{\text{active,VP}}$, thus increasing $\eta_{\text{equipment}}$ and η_{tot}. Using the 2.5 mm-nozzle, the vacuum pump can have a positive effect on wall-plug energy efficiency by inducing improved quenching via supersonic expansion of the plasma effluent.

For the standard configuration, it is clearly the best option to operate at sub-atmospheric pressure where the improved quenching allows for significantly higher conversions and wall-plug energy efficiencies. The highest wall-plug energy efficiency was obtained at 150 mbar with

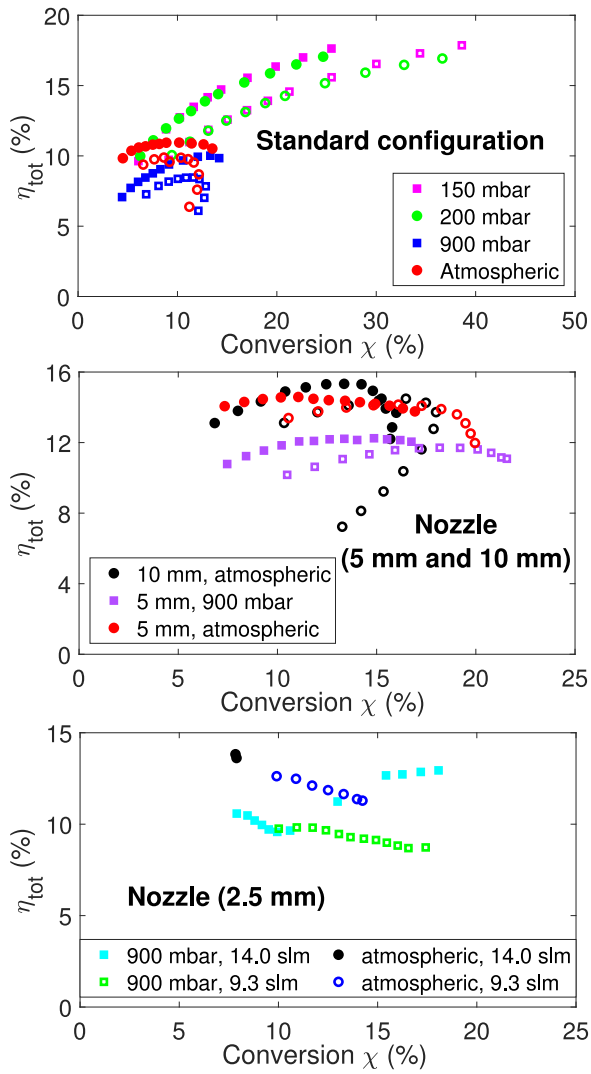

Fig. 12. Wall-plug energy efficiency for the standard configuration and the nozzle configurations at 9.3 slm (empty symbols) and 14.0 slm (filled symbols).

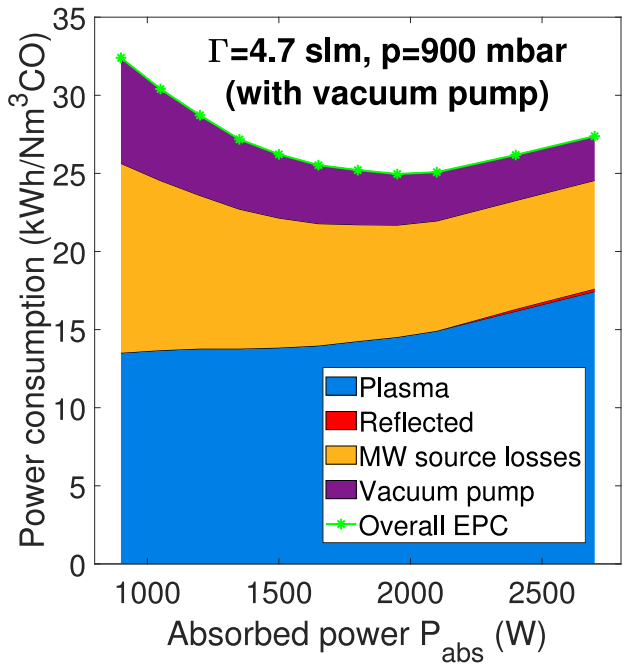

Fig. 13. Electrical power consumption and the different constituents of the power consumption for a plasma in cooling channels configuration.

η_{tot} = 17.9% at a conversion of χ = (38.6 ± 1.6)%. Therefore, the best performance obtained for standard configuration is very similar to the best performance obtained in the cooling channels configuration at atmospheric pressure with identical maximum wall-plug energy efficiency of η_{tot} = 17.9%. In both cases, the best performance was obtained for an absorbed power of P_{abs} = 2.7 kW, being the highest power used throughout this study.

The above determined wall-plug energy efficiencies allow to compare different plasma sources for CO_2 dissociation with each other based on an industrially relevant parameter, i.e. the total energy efficiency η_{tot}. Since different plasma sources (microwave plasmas, dielectric barrier discharges, gliding arc plasmas, ...) rely on different equipment outside of the plasma itself, one can expect the ratio η_p/η_{tot} to be rather different for different plasma sources. It is thus not sufficient to compare different plasma sources with each other solely based on the plasma energy efficiency η_p, although this is the way how it is done in the vast majority of literature. For microwave plasmas, it is shown in this paper that the inefficiency in the microwave generation can lead to significant energy losses; for example for dielectric barrier discharges, one can expect considerable energy losses from high-voltage generation. It is therefore of uttermost importance to compare different plasma sources also in terms of wall-plug energy efficiency since it is this parameter that most directly influences the operational expenditure of the CO_2 conversion process.

Besides plasma gas conversion, also other technologies have been developed for the conversion of CO_2 such as thermocatalytic conversion and electrochemical conversion (solid oxide electrolysis, molten carbonate electrolysis, low-temperature electrolysis) [7,32]. In particular solid oxide electrolysis cells are already highly developed (technology readiness level 8) with the eCOs™being the first commercially available solid oxide electrolysis system for CO_2 dissociation [32,36]. The wall-plug energy efficiency as defined in Eq. (11) allows also compare these technologies with plasma-based CO_2 dissociation technologies. Thus, the total energy efficiency η_{tot} is a very general parameter allowing for comparison between different CO_2 conversion technologies.

Another parameter that can be used to compare different CO_2 conversion technologies with each other is the EPC, i.e. the active electrical energy (in kWh) that is needed to produce one cubic meter of CO (N m^3 defined at 0 °C and 1013 hPa). As one can see from Eq. (12), the EPC is directly proportional to η_{tot}^{-1}. However, the EPC yields more insight into the different energy loss channels since the power consumptions required by the different channels are additive (see Fig. 13).

Fig. 13 shows the overall electric power consumption as well as the different constituents of the power requirement for a power scan performed in the cooling channels & reverse vortex configuration. For this power scan, one observes a minimum electric power consumption of EPC = 25.0 kWh/N m^{3}CO at an absorbed microwave power of P_{abs} = 1950 W, corresponding to a maximum in η_{tot} in Fig. 11. The existence of this minimum in EPC can be explained by considering the different contributions to the EPC: Since plasma becomes less energy efficient (decreasing η_p) with increasing P_{abs}, the energy requirement of the plasma sub-system per produced N m^3 of CO increases with increasing P_{abs} (see blue area). This unfavorable trend of the plasma sub-system is counteracted by the increase in $\eta_{MW\ source}$ and $\eta_{equipment}$, related to the microwave source and the vacuum pump. As already pointed out in Section 4.1 microwave generation becomes more efficient towards higher injected microwave powers. Also for the vacuum pump, the power requirement per produced N m^3 of CO decreases towards higher P_{abs}. This results in the observed U-shape for the EPC-curve. Note that

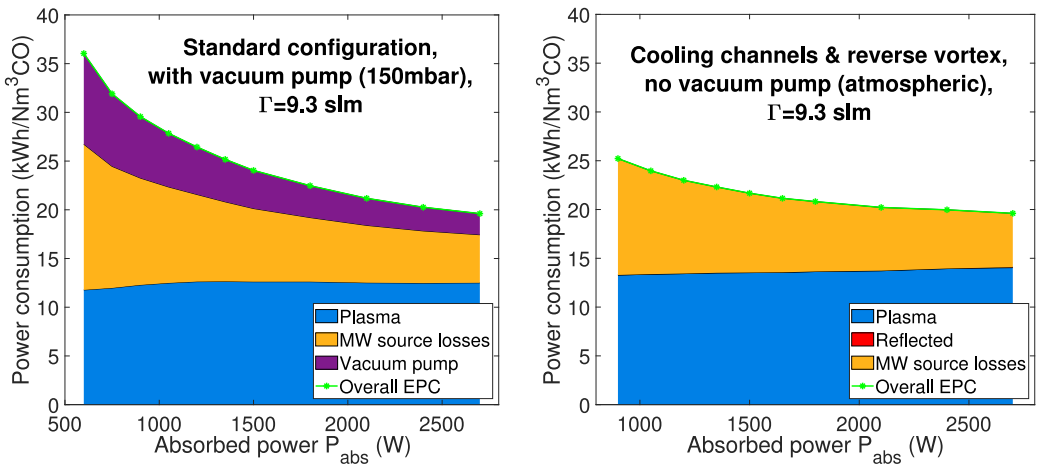

Fig. 14. Electric power consumption and the different constituents of the power consumption for experiments performed with 9.3 slm feed flow rate. For the experiment in the standard configuration, zero reflected power was measured. For the experiment in the cooling channels & reverse vortex configuration, the vacuum pump was disconnected.

the energy losses due to reflection of the microwaves are comparably rather small (in the considered experiment in Fig. 13, even at P_{abs} = 2.7 kW only 27 W of reflected power was measured).

Finally, a comparison of the two setups in which the highest wall-plug energy efficiency of η_{tot} = 17.9% was reached is given in Fig. 14. This η_{tot} was obtained in standard configuration as well as in the cooling channels configuration, in both configurations at P_{abs} = 2.7 kW and a CO_2 feed flow of 9.3 slm. In the standard configuration, this most energetically efficient point was achieved at 150 mbar, whereas in the cooling channels configuration it was obtained at atmospheric pressure operation. Therefore, the plasma energy efficiency η_p is higher (or equivalently, the power consumption of the plasma per produced N m^3 of CO is lower) in the standard configuration than in the cooling channels configuration (compare the blue areas). However, the 150 mbar-operation in standard configuration requires additional power for the vacuum pump (see purple area). This power requirement $P_{active,VP}$ is eliminated completely in the cooling channels configuration by operating at atmospheric pressure. In the end, both configurations end up at the same minimum electric power consumption of EPC = 19.6 kWh/N m^{3}CO. Thus, for industrial application it might be the preferred solution to operate at atmospheric pressure since this saves all maintenance costs as well as capital expenditure related to the vacuum pump without compromising on the total energy efficiency. A modular design for the setup might even further reduce the EPC.

5. Durability

Typical lab experiments reported in literature for plasma-based CO_2 dissociation take only a few hours and never longer than a working day. For industrial application, however, considerably longer operation times of many years, or potentially even decades, are required. Furthermore, it is important that maintenance and repair times during the lifespan of the system are limited. For electrochemical CO_2 conversion, many durability tests are reported in literature: Molten carbonate electrolysis cells were tested for 100–120 h, low-temperature electrolysis cells for up to 4380 h and solid oxide electrolysis cells up to 7600 h [32]. However, except for a rather short stability test for plasma-catalytic CO_2 dissociation over 150 min [37], to our knowledge, no durability test has been published so far for CO_2 decomposition via microwave plasmas.

Here, we report on a first-of-a-kind durability test for the plasma torch with an operation time of 29 h and 20 min. In accordance with the basic idea of Power-to-Gas technologies to utilize temporary surpluses of electrical energy from intermittent renewable sources to produce valuable gases, plasma operation was not continuous, but divided into four blocks of operation. The experiment was performed in the cooling channels & reverse vortex configuration at a CO_2 gas flow of 10.2 slm and an absorbed power of P_{abs} = 2.25 kW. In the experiment, the vacuum pump was only used to facilitate ignition, and it was disconnected after a start-up time of 2–3 min.

Fig. 15 shows the most important figures of merit during the durability test. One observes that the microwave plasma system yields highly reproducible results across several days of measurement. The plasma system is also very stable in all figures of merit (the initially somewhat lower conversion on the first day of measurement is assigned to an incomplete bake-out of the mass spectrometer). This is quite an advantage over low-temperature electrolysis cells for which the performance can fluctuate over time quite significantly [32]. Furthermore, switch-on times of the plasma are very short (2–3 min) and stable operation at highest energy efficiency is obtained almost immediately. This is quite an important characteristic of plasma-based CO_2 dissociation which makes it well-suited to be used as a Power-to-Gas technology that utilizes electricity from intermittent renewable energy sources such as wind and photovoltaics.

6. Impurities in the feed gas

In the above described lab-scale experiments, carbon dioxide was drawn from gas bottles that deliver the CO_2 with a purity of grade 3.5, i.e. ≥99.95% CO_2. For industrial-scale application of CO_2 conversion, one can expect comparably rather impure streams of CO_2 entering the reactor, depending on the source of the carbon dioxide. David W. Keith et al. [38] describe a process for direct air capture (DAC) of carbon dioxide based on absorption of CO_2 in an aqueous potassium hydroxide solution. Nitrogen and oxygen can enter the process through the calciner such that the total process provides an atmospheric pressure CO_2 stream with about 1.36% O_2, 1.51% N_2 and 0.01% H_2O. Direct air capture by adsorption yields an impurity concentration (O_2, N_2 or also H_2O) of ≤1% [39]. A worst-case scenario is given by an oxy-fuel combustion process which provides CO_2 with rather high impurity concentrations of 0%–5% Ar, 0%–15% N_2, 0%–7% O_2 and 0–1.5% SO_2 after the moisture removal unit [40].

For plasma-based CO_2 dissociation, already small amounts of impurities in the CO_2 feed gas can have a rather large effect on the performance as shown by R. Snoeckx et al. [17] for a dielectric barrier discharge: increasing the nitrogen admixture from 0% to 1% results in a steep jump upwards in effective CO_2 conversion from 3% to 4%, i.e. around 30% more of the CO_2 is converted. Moreover, it was shown by Heijkers et al. [41] that in a surfaguide driven by 915 MHz microwaves, effective CO_2 conversion and energy efficiency decrease

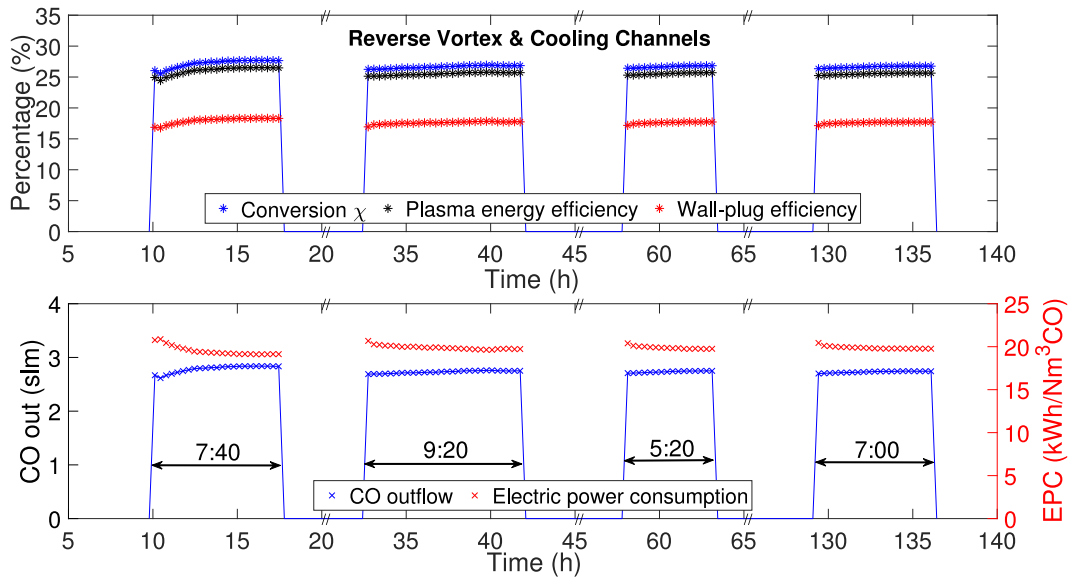

Fig. 15. Time traces of the most important figures of merit for the durability test. Data from the durability test is available as a supplementary material.

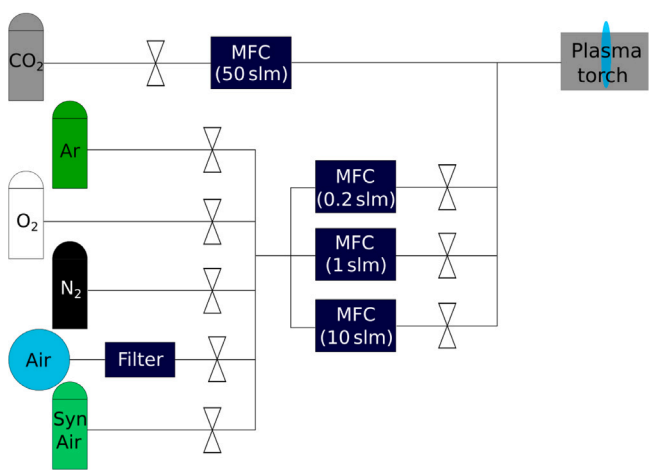

Fig. 16. Experimental setup for testing the influence of impurities.

Table 2
Overview of the admixed gases and their purities.

Gas	Purity
Argon	≥99.998%
Nitrogen	≥99.999%
Oxygen	≥99.5%
Compressed air	–
Synthetic air	≥99.9999%

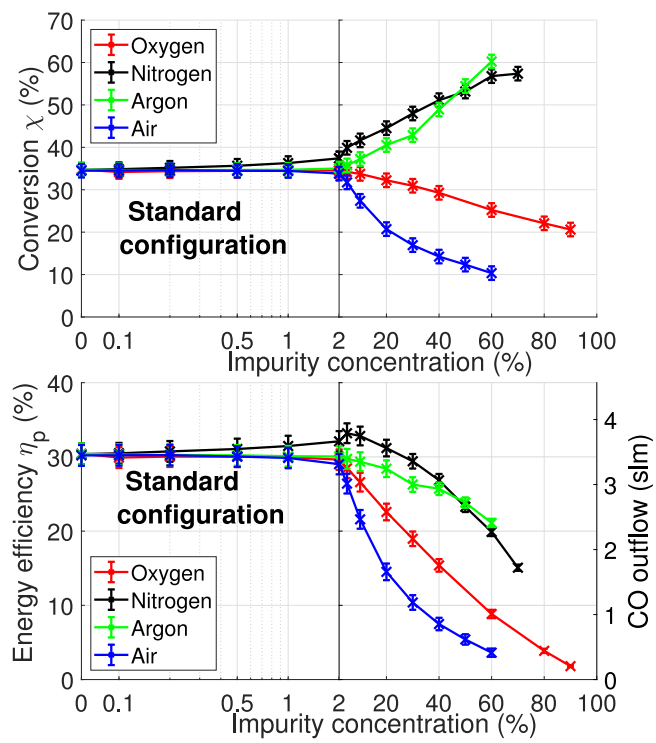

Fig. 17. Effect of impurity N_2, Ar, O_2 and compressed air on conversion and plasma energy efficiency in the standard configuration at 200 mbar. Note the transition from log scale to linear scale at 2% impurity concentration.

only minimally upon N_2 admixtures of up to around 60%. This is caused by an increase in absolute CO_2 conversion that compensates for the lower fraction of CO_2 in the gas stream. Thus, it is of high importance to know the effect of potential impurities on the conversion of carbon dioxide in a microwave plasma torch.

To investigate the effects of impurities on CO_2 conversion, high purity CO_2 (grade 5.5, i.e. ≥99.9995% CO_2) is intentionally diluted with argon, nitrogen, oxygen, compressed air (directed through two filters) and synthetic air (see Fig. 16 for the experimental setup and Table 2 for the purities of the dilution gases). A combination of three mass flow controllers was employed for injecting the impurities to be able to precisely achieve low impurity concentrations down 0.1% and high concentrations up to 90%. Experiments were performed in standard configuration at an absorbed power of P_{abs} = 2.4 kW and a fixed total flow of $\Gamma_{CO2} + \Gamma_{impurity}$ = 10.0 slm (see Figs. 17 and 18 for the results) and in the 5 mm-nozzle configuration at an absorbed power of P_{abs} = 1.5 kW and a fixed total flow of $\Gamma_{CO2} + \Gamma_{impurity}$ = 7.5 slm (see Fig. 19 for the results).

In both configurations, one observes a significant increase in conversion χ with increasing nitrogen content in the feed gas stream. For nitrogen concentrations ≤5%, the enhanced conversion χ over-compensates the reduced fraction of CO_2 in the input gas stream,

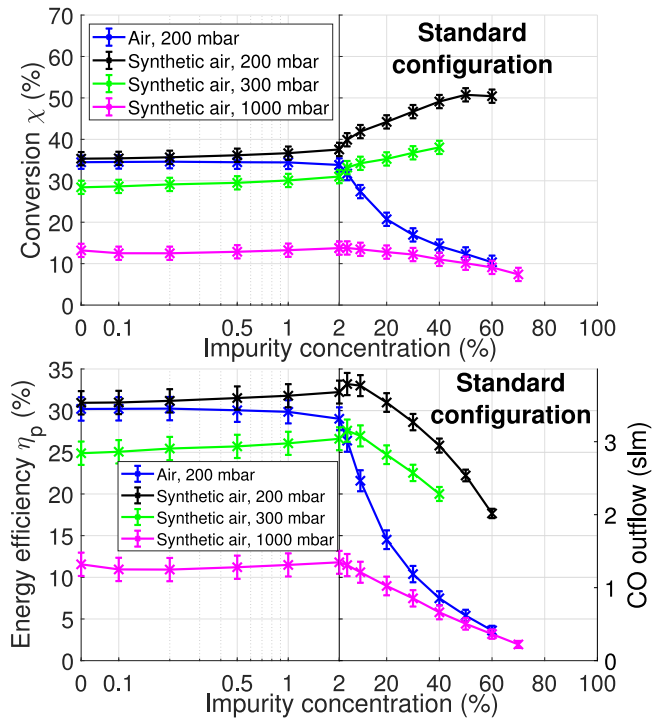

Fig. 18. Effect of compressed air and synthetic air as impurity on conversion and plasma energy efficiency in the standard configuration. Note the transition from log scale to linear scale at 2% impurity concentration.

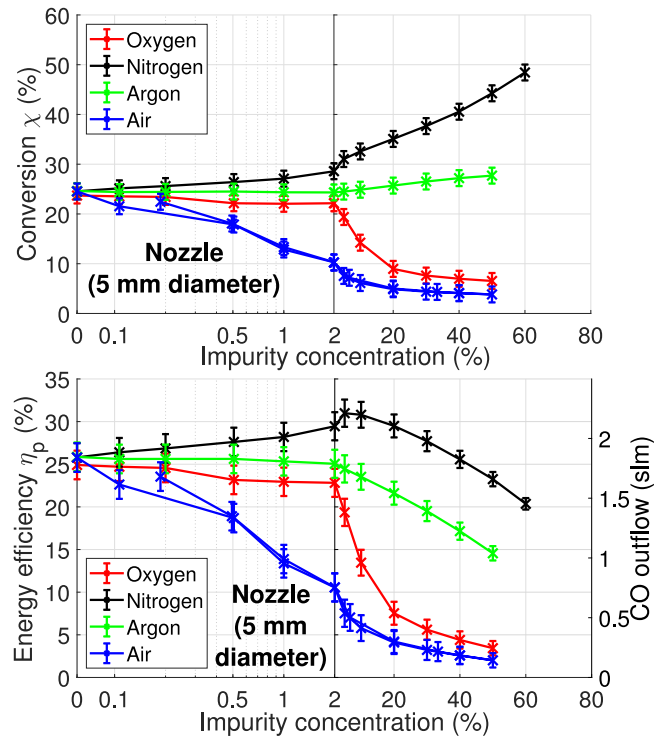

Fig. 19. Effect of impurity N_2, Ar, O_2 and compressed air on conversion and plasma energy efficiency in the 5 mm-nozzle configuration at atmospheric pressure. Note the transition from log scale to linear scale at 2% impurity concentration.

resulting in maximum plasma energy efficiency at a nitrogen concentration of 5% (η_p = (33.2 ± 1.4)% in standard configuration and η_p = (31.0 ± 1.6)% in nozzle configuration). Also for Ar admixture in the feed gas stream, one observes in both configurations an enhanced CO_2 conversion, but a monotonous decrease in energy efficiency. Oxygen as an impurity admixture leads to reduced conversion χ as well as plasma energy efficiency η_p. The most detrimental effect on conversion is observed for addition of compressed air to the input gas stream, in particular for the 5 mm-nozzle. In the standard configuration, already 2% of air lead to a reduction in conversion by one percentage point down to χ = (33.8 ± 1.6)%; in the 5 mm-nozzle configuration, 2% of air even lead to a reduction of 14 percentage points down to χ = (10.3 ± 1.6)%.

An enhancement of CO_2 conversion χ resulting from nitrogen admixture was also observed by A. Indarto et al. in a gliding arc discharge [22,23] and R. Snoeckx et al. in a cylindrical DBD reactor [17]. There are several effects that can contribute such an increased conversion: On the one hand, small amounts of NO_x form in the plasma torch, thereby reducing the amount of oxygen that is available to recombine with CO to form CO_2. On the other hand, electronically excited metastable $N_2(A^3\Sigma_u^+)$ molecules can participate in the dissociation of CO_2 via the reaction $N_2(A^3\Sigma_u^+) + CO_2 \rightarrow CO + O + N_2$. Nitrogen excited into the meta-stable state $N_2(a')$ might contribute as well to the enhanced χ.

An increased CO_2 conversion accompanied by a reduced energy efficiency (due to the reduced effective conversion) was not only observed in our investigations for a microwave plasma torch, but also by Shaojun Xu et al. [42] for a packed-bed non-thermal plasma reactor with 80% argon admixture. A possible explanation might be that argon admixture introduces Ar^+ as a new reaction partner into the system. The exothermic charge exchange reaction between CO_2 and Ar^+ can lead to an enhanced amount of CO_2^+ ions which in turn can result in enhanced conversion via dissociative recombination reactions ($e^- + CO_2^+ \rightarrow CO + O$).

A decrease in conversion upon admixture of oxygen to the feed gas stream was also observed for gliding arc plasmas [22,23]. Observing a reduced conversion χ and plasma energy efficiency η_p also for the plasma torch when oxygen is introduced as an impurity admixture is not very surprising, since oxygen addition to the input gas stream fosters recombination reactions of carbon monoxide with oxygen back to CO_2. It shall be noted here that the negative effect of oxygen is considerably more severe in the 5 mm-nozzle configuration at atmospheric pressure (see Fig. 19) than in the standard configuration at 200 mbar (see Fig. 17). This is explained by the presence of ideal quenching at 200 mbar in the standard configuration, minimizing the amount of back-reactions, whereas in the 5 mm-nozzle at atmospheric pressure, quenching takes place on longer time scales (see discussion in Section 3), leaving more time for recombination reactions to occur.

Observing the most detrimental effect upon compressed air admixture is interesting given the fact that the major components of air (78% nitrogen, 21% oxygen and 1% argon) all led to a less negative effect on CO_2 conversion. The strong negative effect of air on CO_2 dissociation may be explained by the humidity, i.e. H_2O, in ambient air. Results obtained with synthetic air injection underpin this hypothesis (see Fig. 18): While for real air, a steep decrease in χ and η_p is observed with increasing impurity content, adding synthetic air (mixture of nitrogen and oxygen with a water content of less than 0.5 ppm) to the feed gas flow even leads to increased CO_2 conversion χ.

The molar concentration of H_2O in air can be estimated to be 0.5 mol_{H2O} per cubic meter of air, i.e. about 1% of the molecules in ambient air is H_2O. This means that an air concentration of 1% in the feed gas stream corresponds to an H_2O concentration of about 0.01% in the CO_2 inflow. Regarding the results obtained in the nozzle configuration, one can expect that already 0.02% of water in the feed gas stream leads to a reduction in conversion by around 14%.

As a result, this raises the necessity for industrial-scale application to operate the plasma torch with absolutely dry carbon dioxide, i.e. CO_2 gas with not more than about 100 ppm of water impurity. If the CO_2

is provided with some amounts of moisture in the gas (as it is the case in direct air capture and also oxy-fuel combustion), there is the requirement for an additional drying unit that is placed in front of the plasma torch and that removes all water from the input gas stream.

7. Conclusions

A comprehensive study on the wall-plug energy efficiency, durability and impurity impacts is reported for microwave plasma torches for CO_2 conversion. An energy meter system was implemented to monitor the electrical power requirements of the major electricity consumers, being the microwave power supply and the vacuum pump. The wall-plug energy efficiency (η_{tot}) and the electric power consumption (EPC) have been introduced as new criteria to compare different (plasma-based as well as non-plasma-based) CO_2 dissociation technologies with each other. In particular the EPC influences directly the operational costs in the way that multiplying the EPC with an electricity price directly yields the electricity costs for splitting up one $N\,m^3$ of CO_2. Using the energy metering setup, it was demonstrated that the highest wall-plug energy efficiency that can be obtained with the lab-scale microwave plasma torch under investigation is $\eta_{tot} = 17.9\%$, corresponding to an electrical power consumption of 19.6 kWh per produced $N\,m^3$ of carbon monoxide.

There are two ways to achieve this point of maximum wall-plug energy efficiency both of which rely on suppressing the recombination reactions of CO and oxygen back to CO_2: Employing a vacuum pump, one can make use of the ideal quenching that appears at sub-atmospheric pressure operation in the standard configuration. Alternatively, the cooling channels configuration can be used for rapid quenching, which allows to obtain this point of maximum energy efficiency even at atmospheric pressure. For industrial-scale operation, this might be the preferred solution since atmospheric pressure operation allows to omit the vacuum pump, thus reducing CAPEX as well as maintenance-related OPEX. However, ignition of a CO_2 plasma at atmospheric pressure is still a problem in the plasma torch when the tip of the ignition pin is already blunted after long operation. Other more reliable concepts for ignition need to be identified and tested, like for example an initial ignition phase with Ar.

It shall be mentioned explicitly here again that the investigated microwave plasma torch is a lab-scale device, not optimized for industrial application. Nevertheless, this investigation yields valuable insights in view of industrial application. Since the electric power consumption is dominated by the energy requirements of the microwave source and the plasma, one can expect the EPC for an industrial-scale facility to be of the same order of magnitude as the numbers reported in this study. As shown in Section 4.1, magnetron-based microwave generators exhibit highest energy efficiency $\eta_{MW\ source}$ if operated close to their nominal power. Thus, for an optimized system, one needs to first define the power at which the plasma torches shall be operated and then the microwave generators need to be chosen such that their nominal power matches this power. Operation of the microwave generators considerably below their maximum power needs to be avoided in order to ensure high $\eta_{MW\ source}$. Similarly, in case a vacuum pump is to be used, its size and pumping speed also needs to be chosen in accordance with the expected flow rates it has to handle. Separation of the effluent gases is beyond the scope of this manuscript, but a detailed investigation of up-scaling membrane-based oxygen separation can be found in elsewhere [43].

In a 29 h long test, it was demonstrated that the performance of the plasma torch is highly reproducible and stable in all figures of merit. Due to the short ramp-up times (2–3 min) and the possibility to immediately switch off the plasma torch if necessary, the plasma torch is a device that is well-suited to be used only during times when there is a surplus of electricity production, for example caused by sunshine at midday or periods of strong wind.

Small amounts of impurities up to around 2% are acceptable for most impurity species (N_2, Ar and O_2) that can be expected in the CO_2 inflow of the reactor and do not considerably diminish the performance of the plasma torch. However, indications are found that even small amounts of water in the input gas flow might have an enormously negative effect on the CO_2 conversion and energy efficiency. However, if dry CO_2 is provided or the CO_2 is dried sufficiently, microwave plasma torches can be a very promising technology for the dissociation of carbon dioxide.

Abbreviations

ASU: Air Separation Unit
CAPEX: capital expenditure
DAC: direct air capture
eCOs™: electrolytic Carbon Monoxide solution
EPC: electric power consumption fig.: figure
MFC: mass flow controller
MW: microwave
OPEX: operational expenditure
PC: personal computer
ppm: parts per million
R&D: Research and Development
SEI: specific energy input
slm: standard liter per minute
TE: transverse electric
VP: vacuum pump

CRediT authorship contribution statement

Christian Karl Kiefer: Writing – original draft, Visualization, Methodology, Investigation, Conceptualization, Data curation, Formal analysis, Validation. **Rodrigo Antunes:** Writing – review & editing, Conceptualization, Data curation. **Ante Hecimovic:** Writing – review & editing, Conceptualization. **Arne Meindl:** Writing – review & editing, Conceptualization. **Ursel Fantz:** Writing – review & editing, Conceptualization, Supervision.

Declaration of competing interest

The authors declare that they have no known competing financial interests or personal relationships that could have appeared to influence the work reported in this paper.

Data availability

Data on the durability test is available as supplementary material. Further data will be made available upon request.

Acknowledgments

The authors would like to thank Christoph Haindl for his technical help regarding the electrical installation of the energy meters. The photo in the graphical abstract was taken by Axel Griesch. A fruitful discussion with Dr. Andreas Schulz (University of Stuttgart) is thankfully acknowledged as well.

Appendix A. Supplementary data

Supplementary material related to this article can be found online at https://doi.org/10.1016/j.cej.2023.148326.

References

[1] P. Friedlingstein, et al., Global carbon budget 2020, Earth Syst. Sci. Data 12 (2020) 3269–3340.
[2] P. Friedlingstein, et al., Global carbon budget 2021, Earth Syst. Sci. Data 14 (2022) 1917–2005.
[3] P. Friedlingstein, et al., Global carbon budget 2022, Earth Syst. Sci. Data 14 (2022) 4811–4900.
[4] United Nations, Paris Agreement, United Nations Treaty Collection, Paris, 2015.
[5] J. Rogelj, et al., Scenarios towards limiting global mean temperature increase below 1.5 °c, Nature Clim. Change 8 (2018) 325–332.
[6] B. de Haart, et al., Trendbericht technische chemie 2021, Nachr. Chem. 69 (2021) 52–59.
[7] R. Snoeckx, A. Bogaerts, Plasma technology – a novel solution for CO2 conversion? Chem. Soc. Rev. 46 (2017) 5805–5863.
[8] L.F. Spencer, A.D. Gallimore, CO2 dissociation in an atmospheric pressure plasma/catalyst system: a study of efficiency, Plasma Sources. Sci. Technol. 22 (2013) 015019.
[9] W. Bongers, et al., Plasma-driven dissociation of CO2 for fuel synthesis, Plasma Process. Polym. 14 (2017) 1600126.
[10] S. Soldatov, et al., Time-resolved optical emission spectroscopy reveals nonequilibrium conditions for CO2 splitting in atmospheric plasma sustained with ultrafast microwave pulsation, ACS Energy Lett. 6 (2021) 124–130.
[11] K. Wiegers, et al., Determination of the conversion and efficiency for CO2 in an atmospheric pressure microwave plasma torch, Chem. Ing. Tech. 94 (2022) 299–308.
[12] F.A. D'Isa, et al., Performance analysis of a 2.45 GHz microwave plasma torch for CO2 decomposition in gas swirl configuration, Plasma Sources. Sci. Technol. 29 (2020) 105009.
[13] A. Hecimovic, et al., Enhancement of CO2 conversion in microwave plasmas using a nozzle in the effluent, J. CO2 Util. 57 (2022) 101870.
[14] S. Van Alphen, et al., Modelling post-plasma quenching nozzles for improving the performance of CO2 microwave plasmas, Chem. Eng. J. 462 (2023) 142217.
[15] A. Hecimovic, et al., Fast gas quenching of microwave plasma effluent for enhanced CO2 conversion, J. CO2 Util. 71 (2023) 102473.
[16] S. Paulussen, et al., Conversion of carbon dioxide to value-added chemicals in atmospheric pressure dielectric barrier discharges, Plasma Sources. Sci. Technol. 19 (2010) 034015.
[17] R. Snoeckx, et al., CO2 conversion in a dielectric barrier discharge plasma: N2 in the mix as helping hand or problematic impurity? Energy Environ. Sci. 9 (2016) 999–1011.
[18] L.F. Spencer, A.D. Gallimore, Efficiency of CO2 dissociation in a radio-frequency discharge, Plasma Chem. Plasma Process. 31 (2011) 79–89.
[19] A. Huczko, A. Szymański, Thermal decomposition of carbon dioxide in an argon plasma jet, Plasma Chem. Plasma Process. 4 (1984) 59–72.
[20] J. Li, et al., Dissociation of CO2 by thermal plasma with contracting nozzle quenching, J. CO2 Util. 21 (2017) 72–76.
[21] S.-H. Yun, et al., Decomposition and conversion of carbon dioxide into synthesis gas using thermal plasma, J. Ind. Eng. Chem. 3 (1997) 293–297.
[22] A. Indarto, et al., Conversion of CO2 by gliding arc plasma, Environ. Eng. Sci. 23 (2006) 1033–1043.
[23] A. Indarto, et al., Gliding arc plasma processing of CO2 conversion, J. Hazard. Mater. 146 (2007) 309–315.
[24] A.J. Wolf, et al., Characterization of CO2 microwave plasma based on the phenomenon of skin-depth-limited contraction, Plasma Sources. Sci. Technol. 28 (2019) 115022.
[25] A.J. Wolf, et al., Implications of thermo-chemical instability on the contracted modes in CO2 microwave plasmas, Plasma Sources. Sci. Technol. 29 (2020) 025005.
[26] E. Carbone, et al., Analysis of the C2 ($d^3\Pi_g$-$a^3\Pi_u$) Swan bands as a thermometric probe in CO2 microwave plasmas, Plasma Sources. Sci. Technol. 29 (2020) 055003.
[27] A. Fridman, Plasma Chemistry, Cambridge University Press, 2008.
[28] M. Leins, et al., Microwave plasmas at atmospheric pressure, Contrib. Plasma Phys. 54 (2014) 14–26.
[29] A. Schulz, et al., Scalable microwave plasma sources from low to atmospheric pressure, Contrib. Plasma Phys. 52 (2012) 607–614.
[30] A. Hecimovic, et al., Quantitative gas composition analysis method for a wide pressure range up to atmospheric pressure—CO2 plasma case study, Rev. Sci. Instrum. 91 (2020) 113501.
[31] Y.P. Butylkin, et al., Mathematical-modeling of the kinetics of the thermal-decomposition of carbon-dioxide in an electric-arc discharge and quenching of the products, High Energy Chem. 13 (1979) 456–461.
[32] R. Küngas, Review-electrochemical CO2 reduction for CO production: Comparison of low- and high-temperature electrolysis technologies, J. Electrochem. Soc. 167 (2020) 044508.
[33] J. Kopecki, et al., Investigations of a high volume atmospheric plasma torch at 915 MHz, Surf. Coat. Technol. 205 (2011) S342–S346.
[34] S. Hao, A. Papalexopoulos, Reactive power pricing and management, IEEE Trans. Power Syst. 12 (1997) 95–104.
[35] A.D. Papalexopoulos, G.A. Angelidis, Reactive power management and pricing in the California market, in: Proceedings of the 2006 Mediterranean Electrotechnical Conference, 2006, pp. 902–905.
[36] R. Kü, et al., ECOs - A commercial CO2 electrolysis system developed by haldor topsoe, ECS Trans. 78 (2017) 2879–2884.
[37] G. Chen, et al., Plasma assisted catalytic decomposition of CO2, Appl. Catal. B 190 (2016) 115–124.
[38] D.W. Keith, et al., A process for capturing CO2 from the atmosphere, Joule 2 (2018) 1573–1594.
[39] S. Deutz, A. Bardow, Life-cycle assessment of an industrial direct air capture process based on temperature–vacuum swing adsorption, Nat. Energy 6 (2021) 203–213.
[40] H. Li, et al., Impurity impacts on the purification process in oxy-fuel combustion based CO2 capture and storage system, Appl. Energy 86 (2009) 202–213.
[41] S. Heijkers, et al., CO2 conversion in a microwave plasma reactor in the presence of N2: Elucidating the role of vibrational levels, J. Phys. Chem. C 119 (2015) 12815–12828.
[42] S. Xu, et al., CO2 dissociation in a packed-bed plasma reactor: effects of operating conditions, Plasma Sources. Sci. Technol. 27 (2018) 075009.
[43] R. Antunes, et al., Proof of concept for O2 removal with multiple LCCF membranes accommodated in the effluent of a CO2 plasma torch, ACS Sustain. Chem. Eng. 11 (2023) 15984–15993.